Thermal and inertial modes of convection in a rapidly rotating annulus

David Pino, Isabel Mercader, and Marta Net
Departament de Física Aplicada, Mòdul B4, Campus Nord, Universitat Politècnica de Catalunya, 08034 Barcelona, Spain
(Received 4 August 1999)

The nature of the primary instabilities that arise in a fluid contained in a fast rotating cylindrical annulus with slightly inclined plane top and bottom boundaries, radial gravity, and internal heating is numerically analyzed. It is shown that for moderate and high Prandtl numbers, the onset of convection is described by a competition of azimuthal thermal modes with different radial structure, which dominate in different regions of the parameter space. By the combined effect of the inclined ends and rotation, there are modes that are attached to the heated wall and slanted to the prograde direction of rotation, and others which are straight and fill the convective layer. Nevertheless, for very small Prandtl numbers the velocity field of the dominant modes corresponds essentially to the inertial solution of the Poincaré equation, and the temperature perturbation is forced by this velocity field. In addition, a detailed exploration of the critical Rayleigh numbers and precession frequencies of the convective modes versus the radius ratio and the Coriolis parameter, for different Prandtl numbers, is presented.

PACS number(s): 47.27.Te, 47.20.−k, 47.32.−y

I. INTRODUCTION

In many geophysical and astrophysical fluid systems, the global circulation is dominated by the existence of high rotation rates, moderate temperature gradients and, of course, a spherical geometry. The main difficulty in dealing with this problem is the curvature of the layer, since it implies tackling fully three-dimensional computations. For this reason, only in the last decade have significant advances been achieved in this subject.

The first attempts to find the asymptotic dependence of the non-axisymmetric onset of thermal convection in self-gravitating spheres were of [1,2]. In the first paper, the author looked for a normal mode solution of the equations concentrated in a layer close to some cylindrical surface with a symmetric axial velocity about the equatorial plane. According to the same method, in [2] it was shown that the most unstable mode had to be antisymmetric, and the critical Rayleigh number was first corrected. In addition, the author calculated the critical Rayleigh number by assuming that in a Boussinesq fluid under very fast rotating conditions, the motion had to be dominated by the rotation, and consequently the Taylor-Proudman theorem was almost fulfilled in any geometry. Consequently the thermal convection in the sphere was treated as if it were the two-dimensional perturbation of a basic axisymmetric state (thermal wind) of a suitable fast rotating annulus with inclined lids, which cut the sphere at the latitude that minimized the Rayleigh number, i.e. at about 63°. This perturbation method gave rise to critical values different than the general asymptotic theory of [1,2] but described the power dependence correctly. Furthermore, weakly nonlinear calculations of [3] hinted that the critical Rayleigh numbers given by both theories underestimate its real value.

The results were compared with laboratory investigations of the onset of free thermal convection in fast rotating spherical shells and cylindrical annuli [4–6], among others. In both geometries, and in the range of parameters explored, the pattern of convection is columnar. The straight columns are aligned with the axis of rotation and maintain the two-dimensionality, except at their ends, forced by the geometry and/or the boundary conditions. In the experiments, the convection is induced by a radially external heating, and the centrifugal force emulates the gravity field. The small real gravity at first causes the formation of the axisymmetric state, which loses stability by breaking its rotation symmetry. The Spacelab experiment [7] avoided this state, and also confirmed that the theory of [2] at least gives the correct dynamic description of the convective mode. In the space, the gravity was supplied by an electrostatic radial field. All this experimental evidence led to the acceptance of the rotating annulus with radial gravity and inclined lids as the simplest model that retains the main general features of thermal convection in rotating systems.

The 3D numerical computations of [8,9] have also recently revealed some important discrepancies between their own and [1,2] results. The estimation of the asymptotic power-law for the onset of convection at large Taylor numbers bears out the power dependence, but clearly states that the analytical coefficients give rise to critical Rayleigh numbers and precession frequencies of the waves which are under and over, respectively, those given by the numerical ones. In addition, for small Prandt numbers the structure of the marginal modes is not a tall column. If the fluid has a very small Prandtl number, it selects at onset an inertial mode attached to the outer wall, i.e., the pattern of convection will be a short equatorially trapped vortex influenced by the existence of the curved outer boundary. Otherwise, for moderate small Prandtl numbers, the thermal columnar rolls, by effect of the curvature and of the rotation, can spiral from the 63° latitude to the equatorial region, also departing from the annular constraint.

The disagreements at moderate small Prandtl numbers were explained by the revised asymptotic theory of thermal convection in rapidly rotating systems of [10]. In this paper the author used a unified formulation for self-gravitating geophysical and centrifugal-force-driven laboratory systems in the limit of weak inclination of the outer boundaries rela-

tive to the equatorial plane. He demonstrated that the separated formulations are identical at leading order, but at next order differ in a term that depends on the Prandtl number. The formulation leaves aside the outer trapped modes, and consequently agrees very well with [8] results. However the asymptotic limit starts to fail for Prantdl numbers less than 0.1.

The model of the cylindrical annulus with oppositely sloping top and bottom boundaries, and heated from the outside, has been extensively used by Busse and co-workers for understanding some dynamical features observed in the atmospheres of Jupiter and Saturn, such as the band structure of the major planets, and in general the dynamic of fast rotating systems. They use the small gap approximation, and by a perturbation method find a quasi-geostrophic solution bifurcating from the purely radial conduction state that exists if the ends of annulus are only slightly inclined. In this paper, we make use of a similar model, but retain the curvature of the side walls breaking the mid plane symmetry introduced by the previous approximation. Because of this symmetry breaking we are able to find spirally marginal modes of thermal convection in annular geometry.

The rest of the paper is organized as follows. In Sec. II we introduce the formulation of the mathematical problem and the numerical method used to solve it. In Sec. III we analyze the dissipationless problem and, wherever possible, the marginal convection modes are identified with the dominant diffusive modes found in Secs. III A, III B, and III C for Prandtl numbers 0.7, 7, and 0.025, respectively. Finally, the paper closes with a discussion about our own and related results, and a summary of the results obtained in this paper.

II. MATHEMATICAL MODEL AND NUMERICAL METHOD

We consider an annulus which is rotating about its axis of symmetry with angular velocity $\mathbf{\Omega}$. The gap width is $d \equiv r_0 - r_i$, where r_i and r_0 are the inner and outer radii, and $L(r)$ is the height of the layer, which is supposed to decrease outwards with an angle φ, which is constant with respect to the horizontal plane. The geometric parameters of the problem are the radius ratio $\eta \equiv r_i/r_0$, the aspect ratio $\beta \equiv L_0/d$, where L_0 is the mean height, and $\gamma = \tan\varphi$. The inner and outer side walls are maintained at constant temperatures T_i and T_0, respectively, with $T_i > T_0$, and thermally insulating boundary conditions at the top and bottom ends are adopted

$$\gamma \partial_r T \pm \partial_z T = 0, \tag{2.1}$$

with the plus sign being valid for the top end. The gravity vector $\mathbf{g}(r)$ is taken radially inwards. For the velocity field, no-slip lateral bounding surfaces

$$u = v = w = 0 \quad \text{on} \quad r = r_i, \; r_0, \tag{2.2}$$

and because we are trying to find a z-independent solution, stress-free ones on the slanted top and bottom ends are imposed,

$$(\gamma \tilde{D} \pm \partial_z) v = 0, \tag{2.3a}$$

$$(-a\partial_z \pm \partial_r) w + (a\partial_r \pm \partial_z) u = 0, \tag{2.3b}$$

$$\gamma u \pm w = 0 \quad \text{on} \quad z = 0, \; L(r), \tag{2.3c}$$

where $a = 2\gamma/(1-\gamma^2)$, $\tilde{D} = \partial_r - 1/r$ and $\mathbf{u} = (u, v, w)$ refers to the velocity field in cylindrical (r, θ, z) coordinates. As in the preceding case, the plus sign is valid for the top bound. In fact, as we will see later, experimental and numerical results prove that this solution also exists in the core of the fluid with the realistic no-slip conditions. If so, according to [2], $\sigma \sin\varphi \gg E^{1/4}$ and the weak vertical circulation generated in the Ekman layers and confined near them can be neglected. In the inequality, E is the Ekman number and σ the Prandtl number defined below.

If $\gamma \ll 1$, and irrespective of the kinematic boundary conditions at $z = 0, \; L_0$, there exists a basic z-independent conduction state

$$T_c(r) = \Delta T \frac{\ln \dfrac{r}{r_i}}{\ln \eta} + T_i \quad \mathbf{u} = 0,$$

with $\Delta T = T_i - T_0$. The stability of this state will be described nondimensionalizing the Boussinesq Navier-Stokes, mass conservation and energy equations by means of the gap width, the temperature difference between the side boundaries and the thermal diffusion time d^2/κ, where κ represents the thermal diffusivity. These equations, written in the rotating frame of reference, are

$$\sigma^{-1}(\partial_t + \mathbf{u}\cdot\boldsymbol{\nabla})\mathbf{u} = -\boldsymbol{\nabla} p + \nabla^2 \mathbf{u} + \mathrm{Ra}\Theta \hat{\mathbf{e}}_r - 2\sigma^{-1}\mathbf{\Omega}\times\mathbf{u}, \tag{2.4a}$$

$$\boldsymbol{\nabla}\cdot\mathbf{u} = 0, \tag{2.4b}$$

$$(\partial_t + \mathbf{u}\cdot\boldsymbol{\nabla})\Theta = \nabla^2\Theta - \frac{r^{-1}}{\ln \eta}\mathbf{u}\cdot\hat{\mathbf{e}}_r, \tag{2.4c}$$

where Θ refers to the deviation of the temperature with respect to the conduction profile, $T_c(r)$. $\hat{\mathbf{e}}_r$ is the unit vector in the radial direction, and Ra and σ are respectively the Rayleigh and Prandtl numbers defined by

$$\mathrm{Ra} \equiv \frac{\alpha \Delta T g_e d^3}{\kappa \nu}, \quad \sigma \equiv \frac{\nu}{\kappa}.$$

$g_e = \langle |\mathbf{g}(r) - \mathbf{\Omega}\times(\mathbf{\Omega}\times\mathbf{r})| \rangle$ is the effective gravity across the convective layer, which is also assumed to be radially inwards and constant. α is the coefficient of thermal expansion and ν the kinematic viscosity.

In order to eliminate the pressure by using the incompressibility condition, and taking into account the periodicity of the annulus in the azimuthal direction, we assume that

$$\mathbf{u} = f\hat{\mathbf{e}}_\theta + \boldsymbol{\nabla}\times(g\hat{\mathbf{e}}_\theta + \psi\hat{\mathbf{e}}_z) + \boldsymbol{\nabla}\times\boldsymbol{\nabla}\times(\phi\hat{\mathbf{e}}_z). \tag{2.5}$$

The potentials f and g are related with the azimuthal averages of the radial derivatives of the full potentials ψ and ϕ. According to [11,12] the linearized Eqs. (2.4) have been replaced by others written in terms of the velocity potentials

$$(\sigma^{-1}\partial_t - \tilde{\nabla}^2) f = 2\sigma^{-1}\Omega\partial_z g, \tag{2.6a}$$

$$(\sigma^{-1}\partial_t-\tilde{\nabla}^2)\tilde{\nabla}^2 g=-\mathrm{Ra}\partial_z\overline{\Theta}-2\sigma^{-1}\Omega\partial_z f, \quad (2.6b)$$

$$(\partial_t-\nabla^2)\overline{\Theta}=\frac{1}{r\ln\eta}\partial_z g \quad (2.6c)$$

and

$$(\sigma^{-1}\partial_t-\nabla^2)\nabla_h^2\psi=\frac{\mathrm{Ra}}{r}\partial_\theta\Theta+2\sigma^{-1}\Omega\partial_z\nabla_h^2\phi, \quad (2.7a)$$

$$(\sigma^{-1}\partial_t-\nabla^2)\nabla^2\nabla_h^2\phi=\mathrm{Ra}\partial_z D_+\Theta-2\sigma^{-1}\Omega\partial_z\nabla_h^2\psi, \quad (2.7b)$$

$$(\partial_t-\nabla^2)\Theta=-\frac{1}{r\ln\eta}\left(\partial_{rz}^2\phi+\frac{1}{r}\partial_\theta\psi\right), \quad (2.7c)$$

where

$$\nabla_h^2=\frac{1}{r}\partial_r(r\partial_r)+\frac{1}{r^2}\partial_{\theta\theta}^2,$$

$$\tilde{\nabla}^2=\frac{1}{r}\partial_r(r\partial_r)-\frac{1}{r^2}+\partial_{zz}^2,$$

$$D_+=\frac{1}{r}\partial_r(r),$$

$\overline{\Theta}$ being the zero azimuthal mode.

This system has been separated into two parts. The first one (2.6) corresponds to the axisymmetric case, and it shows that a (θ,z) independent velocity and temperature fields are not feasible.

It is known (see [13,14]) that with boundary conditions (2.3), provided that $\varphi=0$ and the rotation rates are high enough, the onset of convection is everywhere z-independent and $w=0$, i.e., convection sets in as a thermal Taylor column. With no-slip top and bottom boundaries, viscous effects are only important in very thin Ekman boundary layers [15], and the flow remains nearly geostrophic. Furthermore, we have already seen that the experimental results [4,6] showed that, with slightly inclined top and bottom ends, $\gamma \ll 1$, the basic pattern of convection can be a columnar azimuthal wave. Thus, we look for a primary quasi-geostrophic solution of Eq. (2.6). For this purpose, as in [16], we split the functions into

$$\psi(r,\theta,z,t)=\psi_0(r,\theta,t)+\tilde{\psi}(r,\theta,z,t), \quad (2.8a)$$

$$\phi(r,\theta,z,t)=\tilde{\phi}(r,\theta,z,t), \quad (2.8b)$$

$$\Theta(r,\theta,z,t)=\Theta_0(r,\theta,t)+\tilde{\Theta}(r,\theta,z,t), \quad (2.8c)$$

where $\tilde{\psi},\tilde{\phi}$ and $\tilde{\Theta}$ are order γ.

Then, at leading order, (2.2) and (2.3) boundary conditions can be written as

$$\psi_0=\partial_r\psi_0=\nabla_h^2\tilde{\phi}=\Theta_0=0 \ \text{ on } \ r=r_i,\ r_0, \quad (2.9a)$$

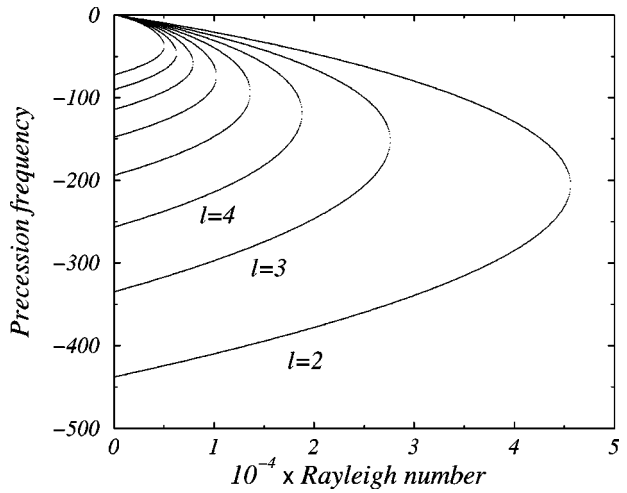

FIG. 1. Marginal stability curves of the dissipationless problem for $\sigma=0.7$, $\tau=5000$, $n=16$, $\eta=0.5$. The value of l indicates the degree of the dominant radial polynomial.

$$\partial_{rz}^2\psi_0=\frac{1}{r}\partial_{\theta z}^2\psi_0=\gamma\frac{1}{r}\partial_\theta\psi_0\mp\nabla_h^2\tilde{\phi}=\partial_z\Theta_0=0 \ \text{ on } \ z=0,\ \beta. \quad (2.9b)$$

The first, second, and fourth conditions of Eq. (2.9b) are identically satisfied and only the third one will be relevant. As is shown in [17], equivalence between (2.4) and (2.7) formulations requires an additional boundary condition at the lateral boundaries, which at leading order is also identically satisfied, $\partial_{rz}^2\nabla_h^2\psi_0=0$, and a gauge condition, $\tilde{\phi}=0$, which, like the third of (2.9a), only appears at higher order. In this case, these conditions are not needed because Eq. (2.7b) does not even appear for the z-independent flow, and the problem can be formulated in terms of a stream function.

By substituting Eq. (2.8) into Eq. (2.7), retaining the leading order terms in the limit of high rotation rates and $\gamma \ll 1$, and averaging over z by using the third boundary condition of Eq. (2.9b), the equations are reduced to

$$(\sigma^{-1}\partial_t-\nabla^2)\nabla_h^2\psi_0=\frac{\mathrm{Ra}}{r}\partial_\theta\Theta_0+\tau\frac{1}{r}\partial_\theta\psi_0, \quad (2.10a)$$

$$(\partial_t-\nabla^2)\Theta_0=-\frac{1}{r^2\ln\eta}\partial_\theta\psi_0, \quad (2.10b)$$

where we have defined the Coriolis parameter

$$\tau\equiv\frac{4\Omega_\nu\gamma}{\beta},$$

and Ω_ν being the rotation rate in viscous units.

The boundary conditions are now

$$\psi_0=\partial_r\psi_0=\Theta_0=0 \ \text{ on } \ r=r_i,\ r_0. \quad (2.11)$$

These equations are solved numerically by expanding the eigenfunction (ψ_0,Θ_0) in the form

$$\psi_0(x,\theta,t)=e^{st}\sum_{m,n}\alpha_{mn}h_m(x)e^{in\theta}, \quad (2.12a)$$

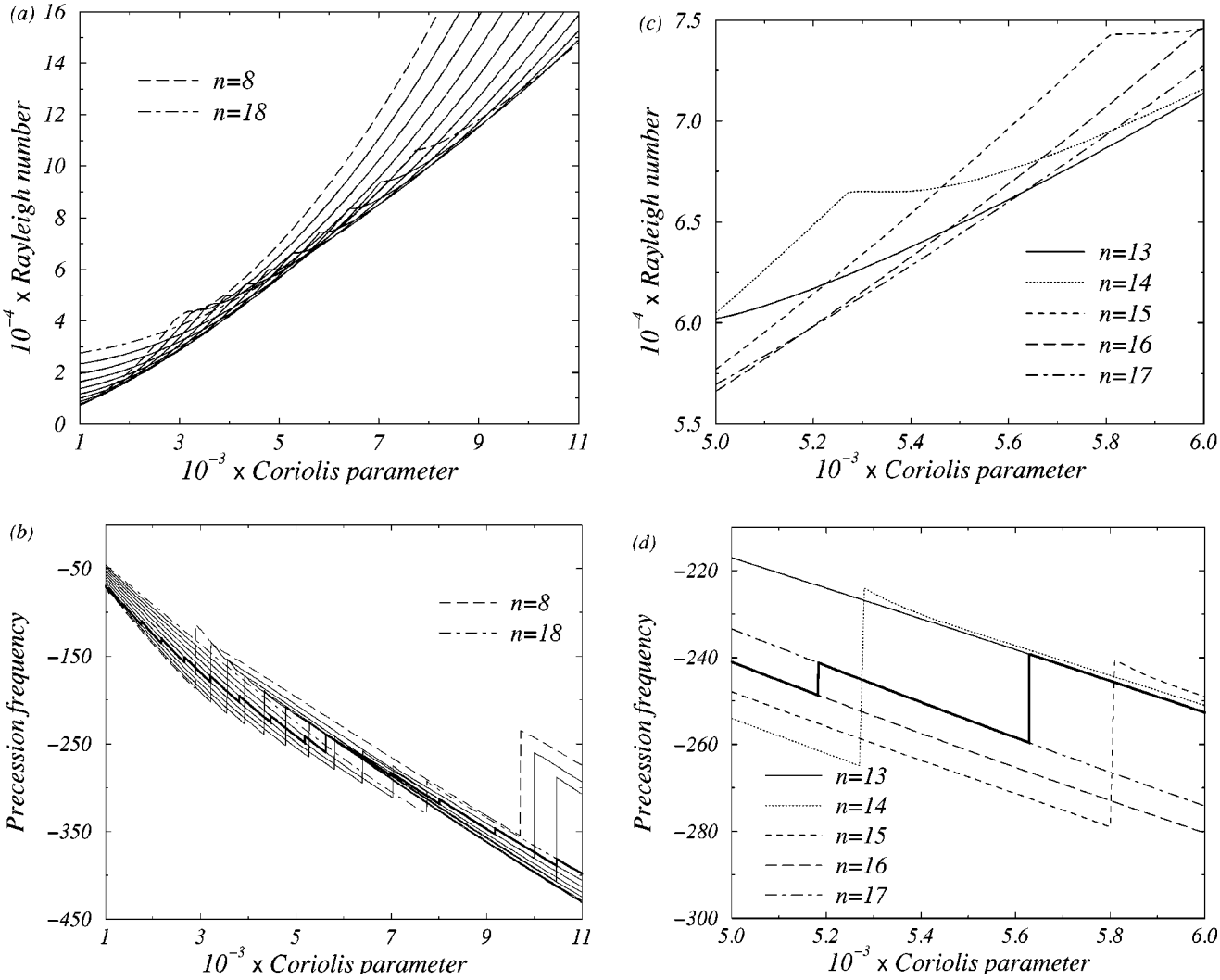

FIG. 2. (a) The critical Rayleigh number, and (b) the corresponding precession frequency as a function of the Coriolis parameter, τ, for $\sigma=0.7$, $\eta=0.5$. (c), (d) are enlargements of the same figure showing the region where the interchange of the two families of dominant modes takes place. The value of n indicates the azimuthal wave number.

$$\Theta_0(x,\theta,t)=e^{st}\sum_{l,n}\gamma_{ln}p_l(x)e^{in\theta}, \qquad (2.12b)$$

where $\mathrm{Re}(s)$ is the growth rate and $\mathrm{Im}(s)$ the precession frequency of the wave, prograde if $\mathrm{Im}(s)<0$ and retrograde if $\mathrm{Im}(s)>0$. The radial coordinate is $x=2r-\delta$, with $\delta=(1+\eta)/(1-\eta)$, and the integers (m,n) and (l,n) indicate the structure of the functions in the radial and azimuthal direction respectively, i.e., $h_m(x)$ and $p_l(x)$ are linear combinations of Tchebyshev polynomials, $T_k(x)$, defined on the interval $[-1,1]$, which verify the boundary conditions. The radial base of the temperature will be

$$p_l(x)=-T_0(x)+T_l(x) \quad \text{if } l\geqslant 2 \text{ even},$$

$$p_l(x)=-T_1(x)+T_l(x) \quad \text{if } l>2 \text{ odd},$$

and that of the stream function

$$h_m(x)=\left(\frac{m^2}{4}-1\right)T_0(x)-\frac{m^2}{4}T_2(x)+T_m(x)$$

if $m\geqslant 4$ even,

$$h_m(x)=\tfrac{1}{8}(m^2-9)T_1(x)-\tfrac{1}{8}(m^2-1)T_3(x)+T_m(x)$$

if $m>4$ odd.

III. RESULTS

The linear stability problem is solved for experimental Prandtl numbers $\sigma=0.025$, 0.7, and 7, and a detailed exploration of these cases is made. All the results are presented with the precession frequencies plotted in viscous units.

In order to identify the physical nature of the solutions that may be present at the onset of convection, Fig. 1 shows the marginal stability curves of the dissipationless problem for a fluid of $\sigma=0.7$, $\tau=5000$, $\eta=0.5$, $n=16$ (the variation of these parameters only gives quantitative changes in the figure). The solutions that are over the curve labeled with $l=2$ correspond to basic solutions dominated by the lower

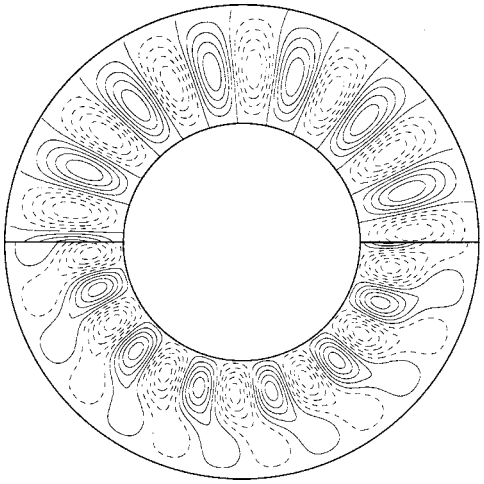

FIG. 3. Contour plots of the temperature perturbation corresponding to dominant modes of the same azimuthal wave number $n=13$ for the parameters $\eta=0.5$, $\sigma=0.7$, (upper half) $\tau=3000$ and (lower half) $\tau=6000$.

order polynomials, $h_m(x)$ and $p_l(x)$ of the expansions (2.12), while the small inner ones belong to solutions dominated by the higher order polynomials $l=3,4,\ldots$, etc. Our waves always travel counterclockwise because of the slope of the boundaries we have chosen.

The upper branch of each curve corresponds to waves whose precession frequency tends to zero when the radial temperature gradient decreases, indicating that they are convective. On the other hand, the frequency of the waves over the lower branches increases when the buoyancy force decreases, until the frequency of the Rossby waves, ω_R, at $\mathrm{Ra}=0$, is reached. Therefore they are inertial waves. The first waves are slow near this point because the buoyancy force almost balances the ageostrophic part of the Coriolis force, and they remain attached near the outer wall. For the second, the main balance is between the ageostrophic force and the quick inertial oscillations, the buoyancy force playing a secondary role. For Rayleigh numbers corresponding to frequencies near $\omega_R/2$, the three terms of the dissipationless equation obtained from (2.10a) are of the same order. If the Rayleigh number is increased, the marginal waves become unstable, and viscosity is needed to dissipate the energy furnished by heating.

Furthermore, we have compared the precession frequency, ω, of the preferred modes of convection found in the dissipative stability analysis [see Fig. 2(b), Fig. 6(b), and Fig. 10(b)] with the frequency, ω_R, of the Rossby waves of the Poincaré equation. Table I contains both frequencies for the dominant n mode that exists at $\tau=5000$, $\eta=0.5$ and every σ explored. Notice that Fig. 1 only gives information about the $\sigma=0.7$ case, because it is plotted for $n=16$. The ω_R values for the other Prandtl numbers have been obtained from the equivalent figures plotted for the dominant modes $n=7$ if $\sigma=0.025$, and $n=17$ if $\sigma=7$. As predicted at this high rotation rate the agreement is very good for small viscous flows, indicating that in low Prandtl number fluids the oscillating modes are mainly of inertial type. A similar result was found by [9] for a spherical shell. By means of a perturbation analysis in the limit of high rotation rates, the author showed that the onset of convection is to leading order an

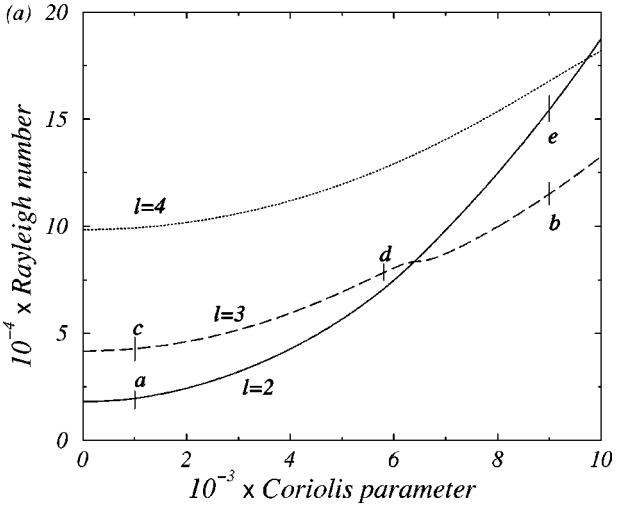

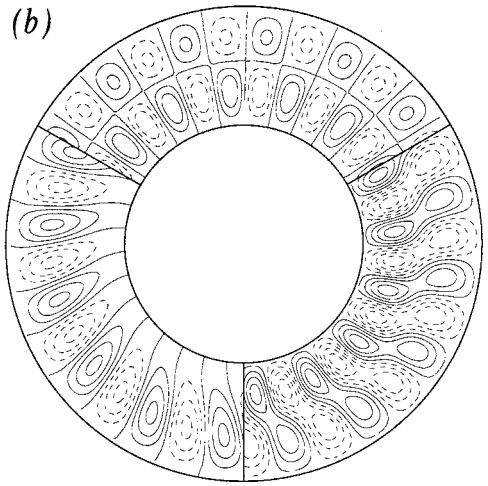

FIG. 4. (a) Marginal stability curves of the first three $n=16$ azimuthal modes with different radial structure for the parameters $\eta=0.5$, $\sigma=0.7$. The solid, dashed and dotted lines correspond to modes with $l=2$, $l=3$, and $l=4$ radial structure, respectively. (b) Contour plots of the temperature perturbation in the c, d, e points labeled in 4(a). In the clockwise direction starting from the top, (first third) $\tau=1000$, (second third) $\tau=5800$ and (third third) $\tau=9000$.

inviscid inertial wave and that the thermal field plays a passive part. At next order it is enough to maintain the wave against viscous dissipation, i.e., the dynamics is induced at onset by the Coriolis term. If $\sigma=0.7$, the frequency of the oscillations is close to $\omega_R/2$. Finally, for higher Prandtl number fluids, the diffusion term becomes of the order of the ageostrophic and buoyancy terms. Then ω_R and ω are very

TABLE I. Comparison of the precession frequencies, ω and ω_R, of the preferred modes of convection for the dissipative and dissipationless problems, respectively. All the frequencies are expressed in viscous units. The parameters are $\tau=5000$, $\eta=0.5$.

σ	ω_R	ω	n
0.025	−730	−678	7
0.7	−437	−241	16
7	−417	−42	17

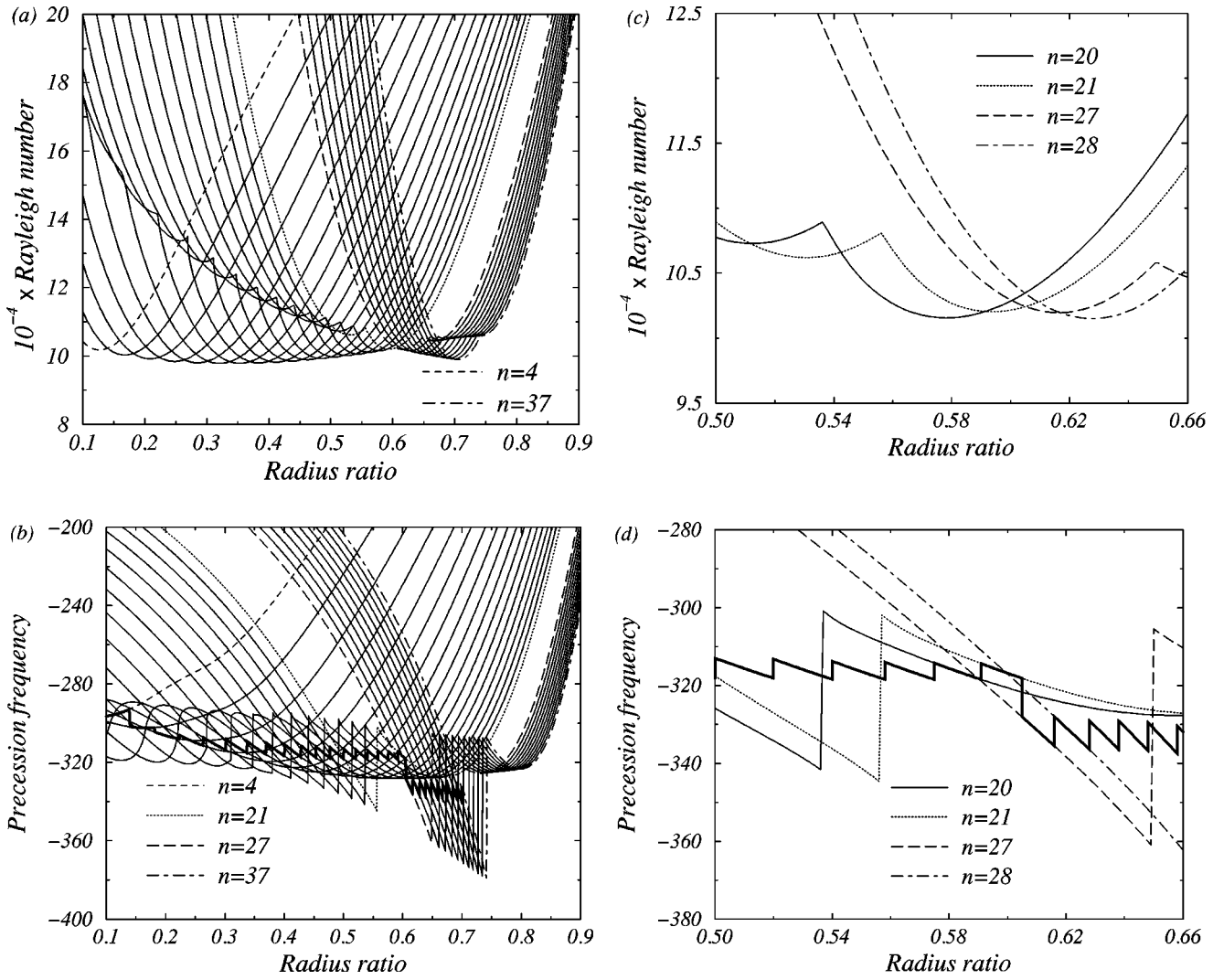

FIG. 5. (a) The critical Rayleigh number, and (b) the corresponding precession frequency as functions of the radius ratio, η, for $\sigma=0.7$, $\tau=8000$. (c), (d) are enlargements of the same figure showing the region where the interchange of the two families of dominant modes takes place. For clarity, only dominant modes have been plotted.

different, and it is not possible to identify the dominant modes of the dissipation problem with those of the dissipationless one. We call the marginal waves that appear at onset for moderate and high Prandtl numbers thermal modes, because both rotation and temperature effects are needed to destabilize the conduction state.

A. Moderate Prandtl numbers

As an example of moderate Prandtl number, we have taken $\sigma=0.7$. Figure 2 displays the Coriolis parameter dependence of (a) the critical Rayleigh number, and (b) the precession frequency for a radius ratio $\eta=0.5$. The labels n indicate the azimuthal wave number, and the heavy line of the frequency curves represents the precession frequency of the dominant solutions at any rotation rate. This notation is followed throughout the paper.

The cusps in the Rayleigh number figure and the jumps between thin lines in the frequency figure are due to changes of each n mode to another of the same azimuthal wave number, i.e., there is a multiplicity of azimuthal modes gathered in families that can dominate for a different range of parameters. In this case, the same family of azimuthal n modes dominates sequentially, and as can be clearly seen in Figs. 2(c) and 2(d), which are enlargements of Figs. 2(a) and 2(b) near $\tau=5500$, there is a family crossing at $\tau=5628$ that produces a backward jump of the dominant azimuthal wave number from $n=17$ to $n=13$. In consequence, there are two solutions with the same wave number $n=13,14,15,16,17$, one of each family, which dominate at different rotation rates. The structure of these modes is shown in Fig. 3, where the contour plots of the temperature perturbation for $n=13$, (upper half) $\tau=3000$ and (lower half) $\tau=6000$ are drawn. The first one is analogous to the solutions found by [18] in the limit of the small gap approximation with the same boundary conditions. In spite of the existence of the Coriolis force, they nearly maintain the reflection symmetry in vertical planes that contain the axis of rotation, i.e., they are connected to the Taylor columns that exist with horizontal lids, $\gamma=0$ (see [13,14]). On the other hand, the second one is a very tilted structure to the prograde direction of the wave and it has clearly broken this reflection symmetry. It can never be found in the small gap approximation, because with this ap-

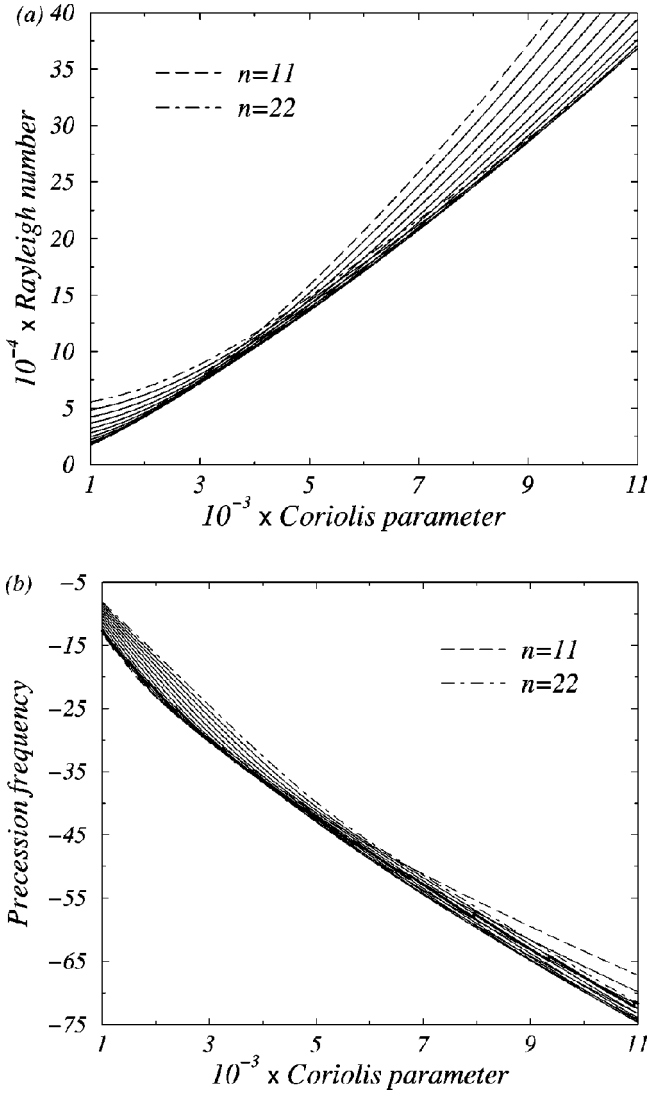

FIG. 6. (a) The critical Rayleigh number, and (b) the corresponding precession frequency as functions of the Coriolis parameter, τ, for $\sigma=7$, $\eta=0.5$.

proach, all the dominant eigenfunctions have a reflection symmetry in the mid plane of the layer. This fact is in agreement with the finding that tilted modes are dominant for higher Coriolis parameters when the radius ratio $\eta\rightarrow 1$. For example, if $\eta=0.7$, the family crossing takes place for $\tau=13367$, but for $\eta=0.3$ it occurs for $\tau=3353$. Another important property of the second family of solutions is that the vortices remain attached to the heated boundary of the annulus. To understand the nature of these dominant modes, we present in Fig. 4(b) the contour plots of the temperature perturbation of the points *c*, *d*, and *e* of Fig. 4(a). This figure shows the Rayleigh number of the three firsts azimuthal $n=16$ modes versus the Coriolis parameter. The solutions labeled as *a* and *b* at $\tau=1000$ and $\tau=9000$ look like those of the upper and lower parts of Fig. 3, respectively. As can be seen in the contour plot of point *c*, the second $n=16$ mode corresponds to a solution dominated by the $l=3$ radial polynomial, which becomes tilted by the effect of rotation (see the contour plot of point *d*), when the rotation rate is increased. Finally, at very fast rotation rates this double columnar pattern is destroyed (see lower part of Fig. 3) and convection remains confined to the inner boundary. By contrast, the contour plot of point *e* shows that the rotation also affects the high *n* solutions with basic radial structure corresponding to $l=2$, but the effect is less spectacular because the radial dependence does not change. In the range of parameters explored, dominant modes with triple layer structure $l=4$ (dotted line) have not been found.

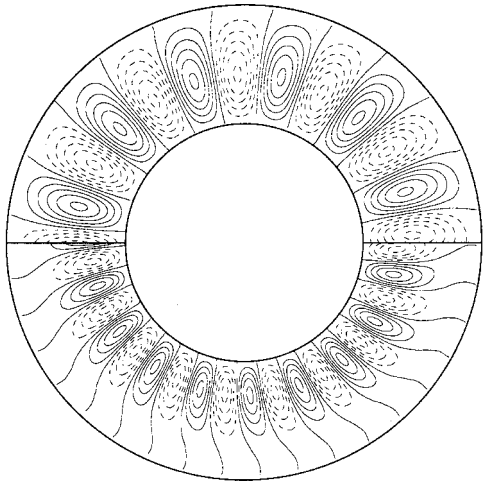

FIG. 7. Contour plots of the temperature perturbation for the parameters $\eta=0.5$, $\sigma=7$, (upper half) $n=14$, $\tau=2000$ and (lower half) $n=20$, $\tau=9000$.

Figure 5 displays the radius ratio dependence of (a) the critical Rayleigh number, and (b) the precession frequency for a Coriolis parameter $\tau=8000$. In these figures, the separation between the central lines is due to the fact that only dominant modes have been plotted. As in the preceding case, (c) and (d) are, respectively, the enlargements of (a) and (b), now around the point $\eta=0.605$, where a forward jump from $n=21$ to $n=27$ is detected, so azimuthal modes $n=22$, 23, 24, 25, and 26 are never dominant. This value has been calculated up to an error of 0.02% and the gap of azimuthal modes is always maintained. For $\sigma=0.7$ and $\eta\geqslant 0.15$, the jumps exist for all the values of τ explored, provided that $\tau\geqslant 2300$, i.e., the smaller the τ is, the smaller the η value for which the forward jump happens. It is important to point out that the preferred modes of convection for $\eta<0.605$ are wall attached and slanted azimuthal modes like those of the lower part of Fig. 3, while if $\eta>0.605$, the preferred modes of convection are straight columns (see the upper part of Fig. 3). Nevertheless, now, depending on the rotation rate, slanted modes can now come from modes with the basic radial structure $l=2$, or from modes with basic radial structure $l=3$ at $\tau\rightarrow 0$. For example, in Fig. 5 dominant $n=4,\ldots,10$ modes come from $l=2$ modes when τ is decreased to low enough values, while dominant $n=11,\ldots,21$ modes are $l=3$ modes at any value of τ. So at $\eta=0.35$ there is also an interchange of solutions, which cannot be easily detected because the plots of the dominant eigenfunctions closely resemble each other. Moreover, at this very high value of τ, there is no multiplicity of the modes $n=4,\ldots,10$ of Fig. 5, but they are continuously changing from an $l=2$ slanted mode to the $l=3$ straight mode, which has to exist for η values near one. In general, at a fixed τ, low *n* slanted modes arise from single changing modes, while high *n* slanted modes are $l=3$ solutions of the prob-

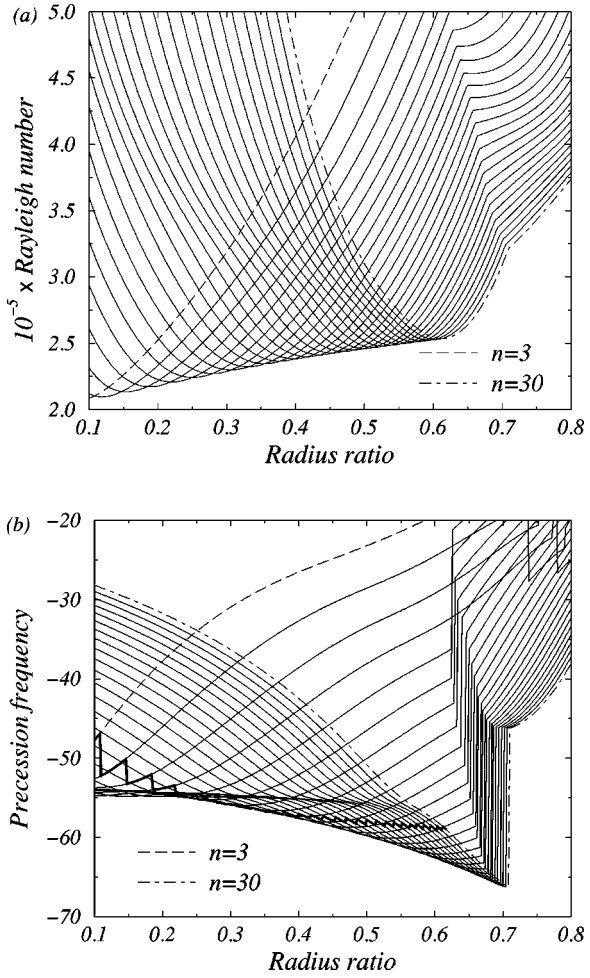

FIG. 8. (a) The critical Rayleigh number and (b) the corresponding precession frequency as functions of the radius ratio, η, for $\sigma=7$, $\tau=8000$.

lem. The results of [19] for a fluid of $\sigma=1$, $\tau=2800$ agree qualitatively well with those for the width gap described above. The authors used the small gap approximation with stress-free side boundary conditions, and expressed the curvature of the end surfaces by means of a point dependent tangent of the angle of inclination of these surfaces $\gamma=\gamma_0[1+\epsilon f(x)]$, where γ_0 is a small constant. With $\epsilon=0.75$, by increasing the wave number, they also found the transformation of the radial structure of a fixed azimuthal mode. This is what they called the switch-over phenomenon.

B. High Prandtl numbers

All the results presented in this subsection correspond to fluids of $\sigma=7$, but we have checked up to $\sigma=100$ that the marginal stability curves plotted versus the Coriolis parameter in Fig. 6(a), and the corresponding frequencies in Fig. 6(b), are essentially the same for all the fluids included in this range of Prandtl numbers. In general, due to the dissipation, the scale of convection is very small, even for an intermediate width of the gap. Now the azimuthal modes dominate, increasing successively from $n=11$ to $n=22$. They have a low precession frequency and always maintain the

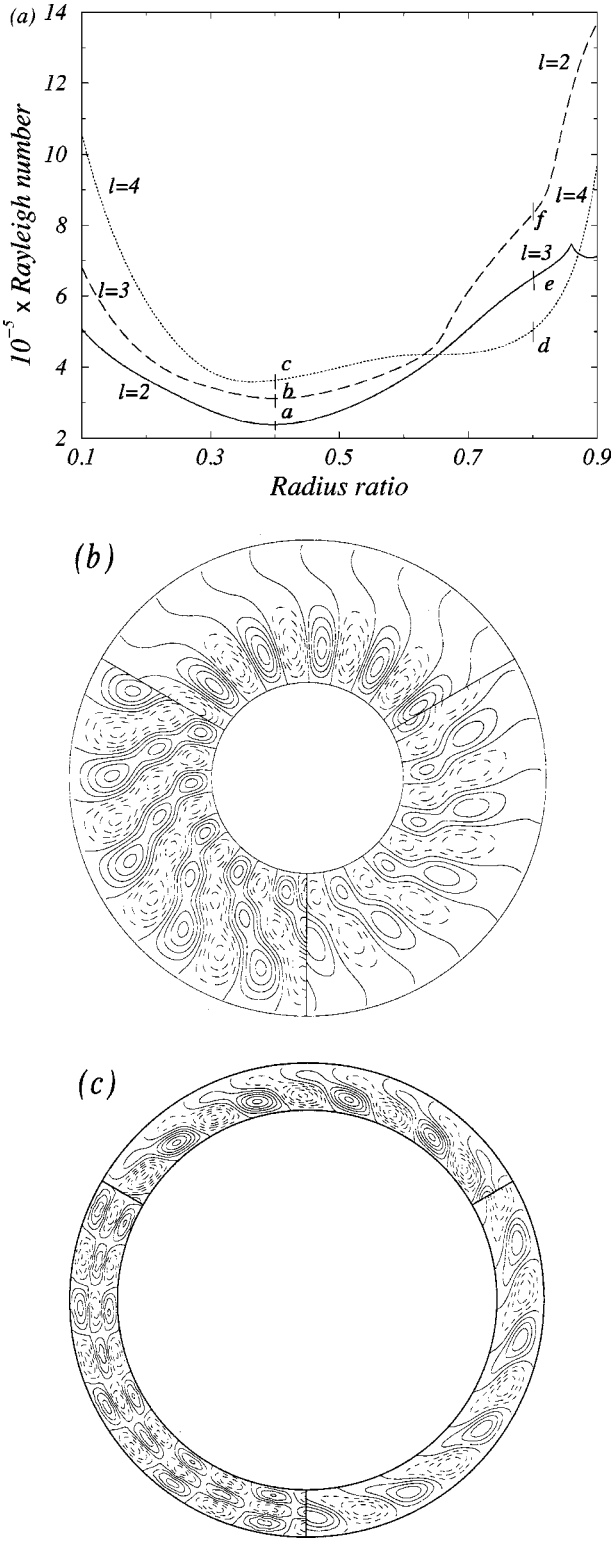

FIG. 9. (a) Marginal stability curves versus η of the first three $n=14$ azimuthal modes with different radial structure for the parameters $\tau=8000$, $\sigma=7$. In a clockwise direction starting from the top, (b) contains the contour plots of the temperature perturbation in the points labeled a, b, and c in $\eta=0.4$ of Fig. 9(a), and (c) those in the points e, f, and d for $\eta=0.8$.

same $l=2$ radial structure. Figure 7 shows the contour plots of the dominant temperature perturbation for $\tau=2000$ in the upper half of the figure and for $\tau=9000$ in the lower half. Now, the differences between both halves are caused just by

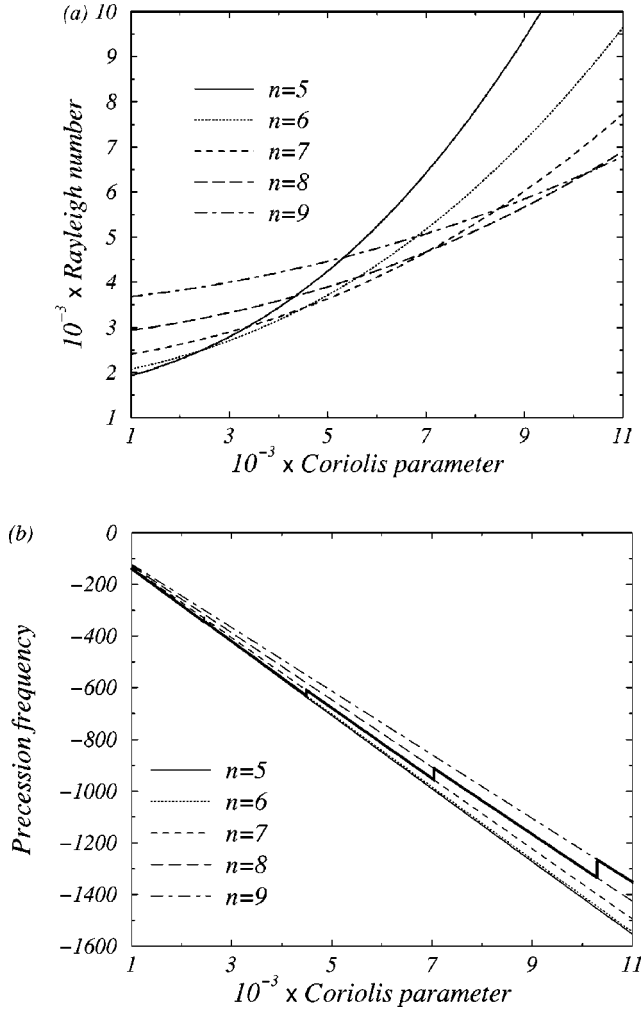

FIG. 10. (a) The critical Rayleigh number, and (b) the corresponding precession frequency as functions of the Coriolis parameter, τ, for $\sigma=0.025$, $\eta=0.5$.

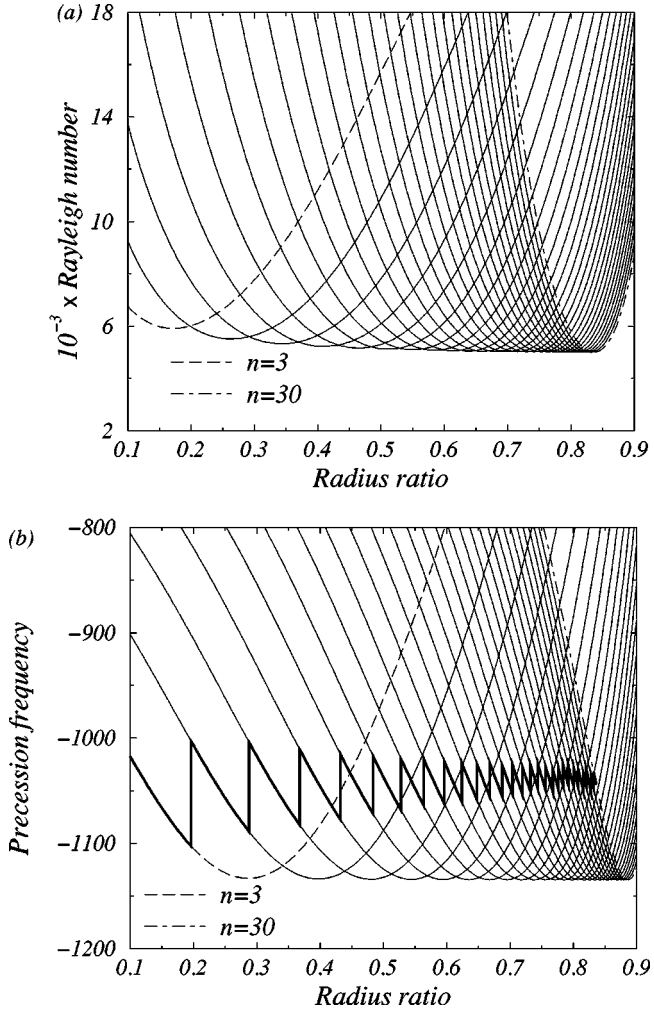

FIG. 11. (a) The critical Rayleigh number, and (b) the corresponding precession frequency as functions of the radius ratio, η, for $\sigma=0.025$, $\tau=8000$.

a continuous increase in the radial phase shift, $\varphi(x)$, and the inner confinement of the amplitude $A(x)$ of the $(l=2, n)$ azimuthal wave

$$\phi_n(x,t)=A(x)\sin[n\theta+\omega t+\varphi(x)],$$

for the highest values of τ. As a result, convection becomes attached to the inner wall and its radial scale tends to be comparable to the azimuthal scale.

In contrast to the preceding case, Figs. 8(a) and 8(b), which display the critical Rayleigh number of the first dominant n modes and their corresponding frequencies versus the radius ratio, show that for narrow gaps the crossing between families of azimuthal modes only drops low enough to suggest that for another Coriolis parameter the second azimuthal mode could be selected at onset. Surprisingly, the contour plot of its eigenfunction makes it clear that it belongs to the $l=4$ radial structure, i.e., it fills the layer forming a triple column. In order to find out what happens with the missing $l=3$ mode, the first three $n=14$ modes are presented in Fig. 9(a) as a function of η. On this figure we have labeled, on the left and right of the curves, the radial structure of every mode at the ends of the interval. The labels of the figure show that the $l=4$ mode maintains its radial structure along the dotted curve. It is preferred for $0.65<\eta<0.87$, but then it is superseded by the solid line of the, at first, $l=2$ mode, which continuously changes to the $l=3$ mode, which in turn exists for $\eta\rightarrow 1$. The cusp in this curve just indicates the zone where the transition has clearly finished. On the other hand, the $l=3$ mode at $\eta=0.1$ transforms into the $l=2$ mode of $\eta\rightarrow 1$. Consequently, it seems very difficult for an $l=4$ radial mode to become dominant at onset in the small gap approximation. These modes become distorted in the same way as the $n=4,\ldots,10$ modes found for $\sigma=0.7$. In order to see this, we present in Figs. 9(b) and 9(c) the contour plots of the six solutions labeled on Fig. 9(a) at $\eta=0.4$ and at $\eta=0.8$, respectively. On the left ($\eta=0.1$), all modes are initially almost straight because $n=14$ is high enough, but the plots of *a* and *e*, placed at the top show that when η is increased, the column attaches to the inner wall and tilts until the double column similar to that of $\sigma=0.7$ is formed. Next, in a clockwise direction *b* and *f* display the opposite change. While the almost existent reflection symmetry in vertical planes is absolutely broken, the inner column starts to diminish. This situation favors the connection of the two vortices and the formation of a single one. The

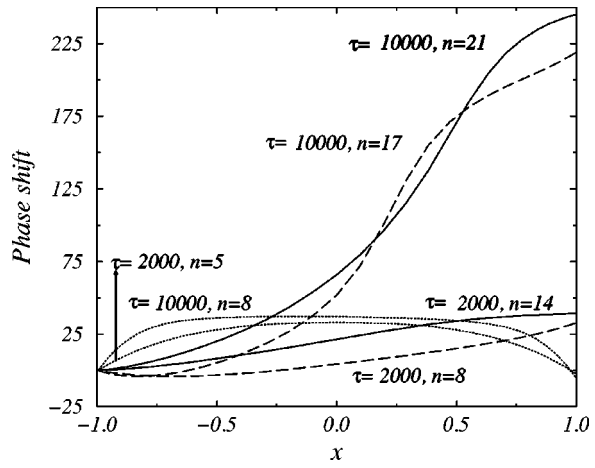

FIG. 12. Radial phase shift of the traveling wave, $\varphi(x)$, for dominant n modes for $\tau=2000$ and $\tau=10000$. The other fixed parameters are $\eta=0.5$ and $\sigma=7$ solid line, $\sigma=0.025$ dotted line, and $\sigma=0.7$ dashed line. The slope of the curves is related to the radial inclination of the columns.

plots of modes labeled c and d show the aforementioned distortion of the $l=4$ radial mode.

As a final clarification, in the same case as $\sigma=0.7$, the low n-modes become slanted at lower rotation rates than the higher ones. So, at $\eta=0.1$ not all the modes are necessarily slanted, as in the case of $\eta\to 1$, where this is imposed by the mid plane symmetry of the layer.

C. Small Prandtl numbers

Figures 10 and 11 display the results obtained with the small Prandtl number $\sigma=0.025$, for the same range of parameters as those in Figs. 2 and 5. We have carefully checked for a wide range of parameters that all the modes correspond to the inertial solutions of the two-dimensional Poincaré equation, and that at any rotation rate or radius ratio they are columns that almost maintain the reflection symmetry in vertical planes, in addition to having the simplest $l=2$ radial structure. As expected, Fig. 10(a) shows that the azimuthal scale of convection is greater for small Prandtl numbers than for moderate ones. This happens because the precession frequency of the waves is so fast that at high rotation rates the frictional forces are not needed for balancing the ageostrophic term of the equation. Beyond their inertial origin, we have not found any similarity between these columnar modes and the equatorially trapped solutions found by [9,20] in rotating spherical shells with internal heating. According to [21], the latter are dominant when $T\lesssim 1.7\sigma^{-4}$, where T is the Taylor number. So for any σ number one can find a rotation rate that gives rise to another form of convection. The condition of three-dimensional convection restricted to low latitudes fails at not very high Taylor numbers; the spiraling columnar mode then becomes dominant. Consequently, the transition from inertial to thermal convection is abrupt. However in annular rotating convection, for a fixed small enough Prandtl number, the same inertial mode is preferred at any rotation rate. Furthermore, as far as we have been able to ascertain, there is a continuous change from one convective mode to another. It seems unlikely that such strong discrepancies could only be due to the different heating, since the inertial wave exists independently of the temperature gradient.

IV. DISCUSSION

We have seen that in a fast rotating annulus, such as in a rotating spherical shell, the onset of convection depends strongly on the Prandtl number. A physical distinction has been made between the hydrodynamic instabilities dominant at small Prandtl numbers and the essentially thermal instabilities dominant at moderate and high σ values.

To summarize the effect of rotation on the dominant modes of convection, we have plotted in Fig. 12 the function $\varphi(x)$, defined in Sec. III B, versus the radial coordinate for some dominant modes of the three Prandtl numbers presented in this paper, at a low and a high Coriolis parameter. The dotted lines of $\sigma=0.025$ are almost constant, except near the side wall, and the slope of those corresponding to $\sigma=7,0.7$ for $\tau=2000$ is so small that in any case the columns nearly maintain the reflection symmetry in vertical planes. For $\tau=10000$, the slope of radial phase shift is $d\varphi(x)/dx\geqslant 1$, indicating that there is a continuous strain from columnar to slanted modes with rotation. This last case fulfills the condition of spiraling columnar convection defined in [8], but according to the asymptotic theory of thermal convection in rapid systems of [10] and to the numerical results of [8], in spherical geometry, the smaller the Prandtl number, the stronger the spiral effect. So the annular approach for the study of convection in self-gravitating bodies makes sense if the onset of convection can be described at onset by columnar not very strong spiral convection. If not, the morphology of the preferred modes and the subsequent dynamics would be completely different. Obviously, the limit of validity depends on the rotation rate.

We have also compared the power laws of the critical Rayleigh number and the precession frequency estimated from our numerical results with

$$\mathrm{Ra}_c=C(\sigma)\tau^{4/3} \quad \text{and} \quad \omega_c=C(\sigma)\tau^{2/3},$$

obtained in [19] for the small gap approximation. With $\sigma=7,0.7$, $\eta=0.5$, we have found a power of 1.26 for Ra_c and one of 0.69 for ω_c, which agree very well with the law. However, with $\sigma=0.025$, the results are 0.76 for Ra_c and 0.89 for ω_c, which differ greatly. We assume that this is because a Rossby wave is in fact a topographic wave, and a small variation in the geometry of the domain has a strong influence on all its characteristics. Whereas a convective roll is caused by a thermal instability, and if the boundary conditions allow the same type of bifurcation, roughly speaking, the geometry only produces minor changes in the coefficients of the power laws and the deformation of the columns. So, the narrow gap approximation and the annular geometry must be used carefully with small Prandtl numbers.

From our own and other published results, we have estimated that for $\sigma\gtrsim O(1)$, the marginal modes of convection are thermal weakly spiraled columns in spherical and annular geometries. For this reason we have presented a detailed description of the radial and azimuthal dependence of the thermal modes with the gap width and the Coriolis parameter. It

is worth pointing out that we have found dominant $l=2,3$ slanted x-modes in the linear regime, and some indications that even the $l=4$ could be dominant for other parameters. With a fixed value of the radius ratio, the spirally modes are preferred at very high rotation rates, while with a fixed rotation rate they are preferred for small radius ratios. Therefore the rotating effect on the large azimuthal scales of convection is stronger.

The competition of azimuthal modes with a non basic radial structure is an indication of the tendency of the fluid to split the convective zone into layers of distinct structure in the nonlinear regime. The linear stability analysis of the nonlinear solutions and the time-dependent evolution of more complex regimes should lead to a better understanding of convection in rotating systems.

ACKNOWLEDGMENTS

This work was supported by DGESIC under Grant No. PB97-0683. Part of the computer time was provided by CEPBA. D. Pino was supported by a FI grant from the DGR of the Generalitat de Catalunya.

[1] P.H. Roberts, Philos. Trans. R. Soc. London, Ser. A **263**, 93 (1968).
[2] F.H. Busse, J. Fluid Mech. **44**, 441 (1970).
[3] A.M. Soward, Geophys. Astrophys. Fluid Dyn. **9**, 19 (1977).
[4] F.H. Busse and C.R. Carrigan, J. Fluid Mech. **62**, 579 (1974).
[5] C.A. Carrigan and F.H. Busse, J. Fluid Mech. **126**, 287 (1983).
[6] M.A. Azouni, E.W. Bolton, and F.H. Busse, Geophys. Astrophys. Fluid Dyn. **34**, 301 (1986).
[7] J.E. Hart, G.A. Glatzmaier, and J. Toomre, J. Fluid Mech. **173**, 519 (1986).
[8] K. Zhang, J. Fluid Mech. **236**, 535 (1992).
[9] K. Zhang, J. Fluid Mech. **268**, 211 (1994).
[10] J-I. Yano, J. Fluid Mech. **243**, 103 (1992).
[11] A. Alonso, Ph.D. thesis, Universitat Politècnica de Catalunya, 1999.
[12] F. Marqués, M. Net, J.M. Massaguer, and I. Mercader, Comput. Methods Appl. Mech. Eng. **110**, 157 (1993).
[13] A. Alonso, M. Net, and E. Knobloch, Phys. Fluids **7** (5), 935 (1995).
[14] G.T. Greed and K. Zhang, Geophys. Astrophys. Fluid Dyn. **82**, 23 (1996).
[15] A. Alonso, M. Net, I. Mercader, and E. Knobloch, Fluid Dyn. Res. **24**, 133 (1999).
[16] F.H. Busse, J. Fluid Mech. **173**, 545 (1986).
[17] F. Marqués, Phys. Fluids A **2** (5), 729 (1990).
[18] M. Schnaubelt and F.H. Busse, J. Fluid Mech. **245**, 155 (1992).
[19] F.H. Busse and A.C. Or, J. Fluid Mech. **166**, 173 (1986).
[20] K.K. Zhang and F.H. Busse, Geophys. Astrophys. Fluid Dyn. **39**, 119 (1987).
[21] A. Tilgner, M. Ardes, and F.H. Busse, Acta Astron. **XIX**, 337 (1997).